12 Density Functional Perturbation Theory and Electron Phonon Coupling

Rolf Heid
Institute for Solid State Physics
Karlsruhe Institute of Technology

Contents

1   Introduction

Electrons and ions are the fundamental building blocks of solids. The understanding of most solid state properties rests on the knowledge of the related quantum objects, electronic quasiparticles and phonons, respectively. Solving the quantum mechanical problem of the electron-ion coupling for extended systems is, however, a formidable task. Still, because of the large mass-difference between electrons and ions, they can be treated to a first approximation as independent dynamical subsystems. In the last decades, highly efficient numerical methods have been developed to solve the electronic part of the problem from first principles. Most of them are based on density functional theory and allow nowadays a routine investigation of the electronic structure of many compounds. The phonon problem took longer to be tackled from first principles, because an accurate solution of the electronic structure is a prerequisite for calculating the fundamental vibrational properties with sufficient accuracy. The development of a linear-response scheme, the so-called density functional perturbation theory, more than 20 years ago opened the door to efficient and accurate approaches and has matured into powerful numerical tools.

The interaction among these constituents, the electron-phonon coupling, influences or even dominates a variety of physical phenomena in solids. This is most noticeable in metals, where low-energy electronic excitations are strongly influenced by lattice vibrations – with important consequences for, e.g., electronic transport and thermodynamical properties. It also represents a natural source for electron pairing underlying the macroscopic quantum phenomenon of superconductivity.

In these lecture notes, I will give an introduction to the basic concepts underlying the modern numerical techniques to calculate phonons and electron-phonon coupling from first-principles within the framework of density functional theory. In Section 2, I will present an overview of the perturbational scheme to calculate phonon properties, and discuss some peculiarities of current implementations. Section 3 is devoted to the first principles approach to the electron-phonon coupling. Connection will be established to experimentally accessible quantities, like quasi-particle renormalization, and to the electron pairing interaction which enters the theory of superconductivity.

1.1   Electron-ion Hamiltonian and adiabatic approximation

We consider a solid to be build up from electrons and ions, where an ion consists of the nucleus and the tightly bound core electrons. The dynamics of electrons and ions in a crystal is described by the total Hamiltonian

$$\mathcal{H} = T_e + V_{ee} + T_i + V_{ii} + H_{e-i}\,, \tag{1}$$

where T_e and T_i are the kinetic energies of electrons and ions, respectively, V_{ee} denotes the Coulomb interaction among electrons, V_{ii} the interaction energy between ions, and H_{e-i} the interaction between electrons and ions.

The task of finding solutions for the Schrödinger equation $\mathcal{H}\Psi(\underline{\mathbf{r}}, \underline{\mathbf{R}}) = \mathcal{E}\Psi(\underline{\mathbf{r}}, \underline{\mathbf{R}})$, where $\underline{\mathbf{r}}$ and

$\underline{\mathbf{R}}$ stand for the set of electron and ion coordinates, respectively, can be drastically simplified due to the large difference of the electron mass m and the ion mass M: The light electrons can be considered as moving much faster than the heavy ions. They follow instantaneously the motion of the ions, while the latter perform small vibrations around their rest positions. As first shown by Born and Oppenheimer [1] for molecules and later applied to solids by Chester and Houghton [2], this picture can be proven by introducing a small parameter $\varkappa$ which scales to 0 for $M \to \infty$. To this end, they considered small displacements of the ions from their rest positions of the form

$$\mathbf{R}_i = \mathbf{R}_i^0 + \varkappa \mathbf{u}_i \,. \tag{2}$$

A proper form for $\varkappa$ can be inferred from the requirement, that the kinetic energy of the ions should be of the same order as the potential term: quadratic in $\mathbf{u}$. This leads to the choice $\varkappa = (m/M)^{1/4}$, which is less than 0.1 for all elements except H and He. One can now perform a systematic expansion of the Hamiltonian and wavefunctions in terms of this small parameter. To lowest order, the total wavefunction can be written as a product $\Psi(\mathbf{r}, \underline{\mathbf{R}}) = \chi(\underline{\mathbf{R}})\psi(\mathbf{r}; \underline{\mathbf{R}})$, where the electronic wavefunction depends only parametrically on the ion coordinates. The electronic wavefunction obeys the equation

$$[T_e + V_{ee} + H_{e-i}(\underline{\mathbf{R}})]\psi_n(\mathbf{r}; \underline{\mathbf{R}}) = E_n(\underline{\mathbf{R}})\psi_n(\mathbf{r}; \underline{\mathbf{R}}) \,, \tag{3}$$

where the dependence on $\underline{\mathbf{R}}$ enters via the interaction H_{e-i}. The ion wavefunction is a solution of

$$[T_i + V_{ii} + E_n(\underline{\mathbf{R}})]\chi(\underline{\mathbf{R}}) = \mathcal{E}\chi(\underline{\mathbf{R}}) \,. \tag{4}$$

This level of approximation is called the adiabatic or Born-Oppenheimer approximation. It describes a decoupling of the dynamics of the electrons and ions and neglects electronic excitations induced by the ionic motion. The electron system enters in (4) via the energies $E_n(\underline{\mathbf{R}})$ of the n-th eigenstate. Usually, one can resort to the ground state and drop the index n, because "normally" encountered excited states at finite temperatures do not deviate much on the scale relevant for the ionic motion. Nevertheless this term includes the important effect of screening of the ionic motion by the valence electrons, which is, however, the same for the ground state as for the excited states.

To go beyond the adiabatic approximation, one uses the solutions of (3) to expand the wavefunction of the solid in the form

$$\Psi_m(\mathbf{r}; \underline{\mathbf{R}}) = \sum_n \chi_{mn}(\underline{\mathbf{R}})\psi_n(\mathbf{r}; \underline{\mathbf{R}}) \,. \tag{5}$$

The eigenvalue problem $\mathcal{H}\Psi_m = \mathcal{E}_m\Psi_m$ leads to the following equation for the ionic part

$$[T_i + V_{ii} + E_n(\underline{\mathbf{R}})]\chi_{mn}(\underline{\mathbf{R}}) + \sum_{n'} \Delta H_{nn'}\chi_{mn'}(\underline{\mathbf{R}}) = \mathcal{E}_m\chi_{mn}(\underline{\mathbf{R}}) \,. \tag{6}$$

The new feature with respect to (4) is the appearance of two additional terms $\Delta H = \Delta H^{(1)} +$

$\Delta H^{(2)}$ given by

$$\Delta H^{(1)}_{nn'} = -\frac{1}{M}\sum_i \int dr^{3N}\,\psi_n^*(\mathbf{r};\underline{\mathbf{R}})\nabla_{R_i}\psi_{n'}(\mathbf{r};\underline{\mathbf{R}})\cdot\nabla_{R_i} \tag{7}$$

$$\Delta H^{(2)}_{nn'} = -\frac{1}{2M}\sum_i \int dr^{3N}\,\psi_n^*(\mathbf{r};\underline{\mathbf{R}})\nabla_{R_i}^2\psi_{n'}(\mathbf{r};\underline{\mathbf{R}})\,. \tag{8}$$

They contain derivatives of the electronic wavefunctions with respect to the ion coordinates, and take into account possible excitations in the electronic subsystem due to the motion of the ions. Among these two non-adiabatic terms $\Delta H^{(1)}$ is typically the dominant one, because from the expansion of ψ_n it contains terms of order $\varkappa$, while $\Delta H^{(2)}$ involves terms of order $\varkappa^2$.
Corrections to $\Psi(\mathbf{r},\mathbf{R})$ beyond the adiabatic approximation can be shown to be of order $\varkappa^3$ and corrections to the energy are of order $\varkappa^6$. The expansion parameter $\varkappa$ only depends on the mass ratio and not on the strength of the electron-phonon interaction. Thus the adiabatic approximation is adequate for both free-electron-like systems and for compounds possessing tighter bound valence electrons like transition metals.

1.2 Phenomenological theory of lattice dynamics

Within the adiabatic approximation, the statics and dynamics of the ions are governed by an effective potential

$$\Omega(\underline{\mathbf{R}}) = V_{ii}(\underline{\mathbf{R}}) + E_0(\underline{\mathbf{R}})\,, \tag{9}$$

where $E_0(\underline{\mathbf{R}})$ denotes the electronic ground-state energy for a given ion configuration $\underline{\mathbf{R}}$. The effective potential Ω builds the starting point of the microscopic theory of lattice dynamics, which has been outlined in a number of review articles [3–5].
Dynamical properties are derived by a systematic expansion of Ω for atom displacements $\mathbf{u}$ around a chosen reference configuration, $\mathbf{R}_i = \mathbf{R}_i^0 + \mathbf{u}_i$, leading to

$$\Omega(\underline{\mathbf{R}}) = \Omega(\underline{\mathbf{R}}^0) + \sum_{i\alpha}\Phi_a(i)u_{i\alpha} + \frac{1}{2}\sum_{i\alpha j\beta}\Phi_{\alpha\beta}(i,j)u_{i\alpha}u_{j\beta} + \dots\,. \tag{10}$$

Greek indices α and β denote Cartesian coordinates, while i and j are atom indices. The term of first order is the negative of the force acting on an atom in the reference configuration

$$F_{i\alpha} = -\left.\frac{\partial\Omega}{\partial R_{i\alpha}}\right|_0 = -\Phi_\alpha(i)\,. \tag{11}$$

It vanishes if one chooses as reference the equilibrium configuration that minimizes Ω. The second-order coefficients are given by

$$\Phi_{\alpha\beta}(i,j) = \left.\frac{\partial^2\Omega}{\partial R_{i\alpha}\partial R_{j\beta}}\right|_0\,. \tag{12}$$

Their physical meaning becomes more evident when one considers the case where only a single ion at site i is displaced from the equilibrium position by $u_{i\alpha}$. Then the force felt by an atom at site j is given by:

$$F_{j\beta} = -\sum_{i\alpha}\Phi_{\alpha\beta}(i,j)u_{i\alpha}\,. \tag{13}$$

Thus, to lowest order, $\Phi_{\alpha\beta}(i,j)$ describes a linear relationship between displacement and resulting force. They are the 3D equivalent of a spring constant and are called harmonic force constants. Higher-order coefficients are denoted as anharmonic force constants. The harmonic approximation is based on truncating the sum after the second order.

In periodic crystals, the atoms are characterized by two indices $i = (l\kappa)$, which denote the unit cell (l) and the atoms inside a unit cell (κ), respectively. For periodic boundary conditions, the Fourier transform of the force constant matrix is related to the dynamical matrix

$$D_{\kappa\alpha\kappa'\beta}(\mathbf{q}) = \frac{1}{\sqrt{M_\kappa M_{\kappa'}}} \sum_l \Phi_{\alpha\beta}(l\kappa, 0\kappa')e^{-i\mathbf{q}(\mathbf{R}^0_{l\kappa} - \mathbf{R}^0_{0\kappa'})}\,, \tag{14}$$

which determines the equation for the normal modes or phonons,

$$\sum_{\kappa'\beta} D_{\kappa\alpha\kappa'\beta}(\mathbf{q})\eta_{\kappa'\beta}(\mathbf{q}j) = \omega^2_{\mathbf{q}j}\eta_{\kappa\alpha}(\mathbf{q}j)\,. \tag{15}$$

$\omega_{\mathbf{q}j}$ and $\eta_{\kappa\alpha}(\mathbf{q}j)$ denote the energy and polarization of the normal mode determined by the wavevector $\mathbf{q}$ and branch index j.

These quantities enter into the relationship between the atom displacements and the usual phonon annihilation and creation operators $b_{\mathbf{q}j}$ and $b^\dagger_{\mathbf{q}j}$ describing quantized normal modes

$$u_{l\kappa\alpha} = e^{i\mathbf{q}\mathbf{R}^0_{l\kappa}} \frac{1}{\sqrt{N_q}} \sum_{\mathbf{q}j} A^{\mathbf{q}j}_{\kappa\alpha}(b_{\mathbf{q}j} + b^\dagger_{-\mathbf{q}j}) \qquad \text{with} \qquad A^{\mathbf{q}j}_{\kappa\alpha} = \frac{\eta_{\kappa\alpha}(\mathbf{q}j)}{\sqrt{2M_\kappa\omega_{\mathbf{q}j}}}\,. \tag{16}$$

A complete characterization of the harmonic vibrational spectrum requires the knowledge of either the normal modes for the whole Brillouin zone, or the force constants for all atom bonds. For a metallic system, the latter representation is often more economical since the lattice interaction in real space is rather short ranged due to electronic screening.

2 Density functional perturbation theory

2.1 Lattice dynamics from first principles

The goal is now to calculate the basic quantities determining the dynamics of the ions. The first term in the effective potential (9) is the Coulomb interaction among the ions, whose contribution to the force constants can be readily obtained. The second term represents the electronic contribution, which incorporates all important physical properties like bonding and screening. It requires a sophisticated and accurate treatment of the electronic system, as provided by density functional theory.

2.1.1 Basics of density functional theory

The foundations of density functional theory (DFT) have been worked out by Hohenberg, Kohn, and Sham [6, 7] in the mid 60's, and are outlined in numerous reviews [8–10]. Here we only mention the essential features which we need later.

In DFT, the ground-state energy of a system of interacting electrons moving in an external potential v_{ext} is obtained by minimizing the functional

$$E[n] = F[n] + \int d^3r \, v_{\text{ext}}(\mathbf{r}) \, n(\mathbf{r}) \tag{17}$$

with respect to the electron density $n(\mathbf{r})$. At its minimum, $n(\mathbf{r})$ is the true electron density of the interacting system. The functional $F[n]$ is universal, i.e. independent of the external potential. For practical applications, the scheme developed by Kohn and Sham has proven to be very useful. They showed that the minimum principle allows us to map the complex many-body problem onto a fictitious system of non-interacting electrons that in its ground state possesses the same inhomogeneous density as the interacting system [7]. They expressed the energy functional as

$$F[n] = T_s[n] + E_H[n] + E_{xc}[n], \tag{18}$$

where T_s represents the kinetic energy of the non-interacting electrons (we adopt Rydberg atomic units defined by $\hbar^2 = 2m = e^2/2 = 1$)

$$T_s[n] = \sum_i f_i \int d^3r \, \psi_i^*(\mathbf{r}) \left(-\nabla^2 \right) \psi_i(\mathbf{r}) \tag{19}$$

and $E_H[n]$ the Hartree energy

$$E_H[n] = \int d^3r \int d^3r' \, \frac{n(\mathbf{r})n(\mathbf{r}')}{|\mathbf{r} - \mathbf{r}'|} \tag{20}$$

with the single-particle representation of the density

$$n(\mathbf{r}) = \sum_i f_i |\psi_i(\mathbf{r})|^2. \tag{21}$$

Here f_i denotes the occupation number of the single-particle state ψ_i. The wavefunctions of the fictitious electrons obey a single-particle equation (Kohn-Sham equation)

$$\left\{ -\nabla^2 + v_{\text{eff}}(\mathbf{r}) \right\} \psi_i(\mathbf{r}) = \epsilon_i \psi_i(\mathbf{r}). \tag{22}$$

The effective potential $v_{\text{eff}}(\mathbf{r})$ is a functional of the density and given as a sum of the external potential and a screening potential

$$v_{\text{eff}}[n] = v_{\text{ext}} + v_{\text{scr}}[n] = v_{\text{ext}} + v_H[n] + v_{XC}[n]. \tag{23}$$

The screening potential is obtained via functional derivatives of the last two terms in the total energy functional (18). It consists of the Hartree potential

$$v_H(\mathbf{r})[n] = \frac{\delta E_H}{\delta n(\mathbf{r})} = \int d^3r' \, \frac{2n(\mathbf{r}')}{|\mathbf{r} - \mathbf{r}'|} \tag{24}$$

which describes an average electrostatic potential originating from the other electrons, and the exchange-correlation potential $v_{XC}(\mathbf{r}) = \delta E_{XC}/\delta n(\mathbf{r})$.

By this formulation, the original many-body problem has been cast into a set of single-particle equations (21)–(23) that has to be solved self-consistently. The complexity of the original many-body problem is transferred to the task of determining the exchange-correlation energy E_{XC}. The big success of DFT partly rests on the empirical fact that already simple approximations to v_{XC} often give very accurate results. The most widely used ansatz is the local-density approximation (LDA)

$$v_{XC}^{\text{LDA}}(\mathbf{r}) = \frac{d(n\epsilon_{XC}^{\text{hom}}(n))}{dn}\bigg|_{n=n(\mathbf{r})}, \tag{25}$$

where $\epsilon_{XC}^{\text{hom}}(n)$ represents the exchange-correlation energy density of the homogeneous interacting electron gas. For $\epsilon_{XC}^{\text{hom}}$ various parametrizations derived from analytical and numerical studies exist [9]. Another popular ansatz is the generalized-gradient approximation (GGA), where in addition to LDA a dependence of v_{XC} on the local gradient of the electron density is considered to better account for inhomogeneous density distributions [11–13].

2.1.2 Application to lattice dynamics

As we have seen in Sec. 1.2, lattice-dynamical properties are determined by the adiabatic lattice potential Ω, which equals the ground-state energy for a fixed ion configuration. Hence, lattice dynamics depends only on ground-state properties of the electronic system, and is accessible in the framework of density functional theory. An overview of the various methods to extract lattice-dynamical properties from *ab-initio* calculations have been given in [14]. One can divide them into two main classes: (i) direct methods and (ii) linear-response techniques.

The direct methods are based on ground-state calculations for the ideal crystal and for geometries with ions displaced from their equilibrium position. The frozen-phonon (FP) technique is conceptually the simplest and historically the first-applied method and uses the quadratic dependence of the total energy from the displacement to extract the frequency of a normal mode [15]. Since this requires *a priori* knowledge of the phonon eigenvector, it can typically be used only in cases where symmetry completely determines its form.

A more efficient scheme employs the linear relationship (13) between an ionic displacement and the forces felt by other ions in the unit cell [16–18]. This can be achieved with little numerical expenses, as forces can be derived directly from quantities obtained in a ground-state calculation with the help of the Hellman-Feynman theorem. A single calculation then gives information about a complete row of the dynamical matrix. The complete dynamical matrix can be constructed using a few appropriately chosen displacements. Hence, this approach does not require any *a priori* information about the normal modes. Since frozen-phonon calculations employ finite displacements of ions, their results principally contain all anharmonic effects, which could be used to extract higher anharmonic coupling constants.

A disadvantage of the direct methods is the need to resort to supercells to extract properties for non-zero wavevector phonons. A complete determination of the phonon spectrum requires supercells with sizes larger than the effective range of the lattice interactions [19–22].

The alternative approach consists of calculating the derivatives of the total energy directly within perturbative schemes. In particular, the dynamical matrix is obtained from the second deriva-

tives via Eq. (12). It has the big advantage that it works directly in reciprocal space and gives access to the dynamical matrix at arbitrary wavevectors without the need for supercells. We will discuss this scheme in some detail now.

2.2   Linear response formulation

Here we show how the perturbative approach is set up within the DFT framework. We will first present some general considerations before applying them to the specific case of perturbations induced by ionic displacements in periodic crystals.

2.2.1   Energy derivatives

Let us consider a situation where the external potential v_{ext} depends on a set of adiabatic perturbation parameters $\Lambda = \{\lambda_a, a = 1, \dots, p\}$. Each v_{ext}^{Λ} determines an electronic ground state with density $n^{\Lambda}(\mathbf{r})$ and total energy $E^{\Lambda} = F[n^{\Lambda}] + \int d^3r \, n^{\Lambda}(\mathbf{r}) v_{ext}^{\Lambda}(\mathbf{r})$, which depends on the perturbation via the external potential and implicitly via the density. Its derivative then contains two contributions

$$\frac{\partial E^{\Lambda}}{\partial \lambda_a} = \int d^3r \, n^{\Lambda}(\mathbf{r}) \frac{\partial v_{\text{ext}}^{\Lambda}(\mathbf{r})}{\partial \lambda_a} + \int d^3r \, \frac{\delta E^{\Lambda}}{\delta n(\mathbf{r})} \frac{\partial n^{\Lambda}(\mathbf{r})}{\partial \lambda_a} \,. \tag{26}$$

Due to the variational principle, the second term vanishes for each finite Λ. Thus the first derivative depends on the ground-state density only. This represents the DFT equivalent of the well known Hellman-Feynman-Theorem [23].

The second-order derivatives are then given by

$$\frac{\partial^2 E^{\Lambda}}{\partial \lambda_a \partial \lambda_b} = \int d^3r \, \frac{\partial n^{\Lambda}(\mathbf{r})}{\partial \lambda_b} \frac{\partial v_{\text{ext}}^{\Lambda}(\mathbf{r})}{\partial \lambda_a} + \int d^3r \, n^{\Lambda}(\mathbf{r}) \frac{\partial^2 v_{\text{ext}}^{\Lambda}(\mathbf{r})}{\partial \lambda_a \partial \lambda_b} \,. \tag{27}$$

For practical purposes it is important that the second derivatives require only the knowledge of the first-order variations of the electron density. Therefore, it is sufficient to consider only the linear response of the electron system.

2.2.2   Linear response within the Kohn-Sham scheme

The linear response within the DFT scheme is obtained by standard perturbation techniques under the condition that the effective potential entering the Kohn-Sham equations depends on the ground-state density itself. Thus its linear variation is given by

$$\delta v_{\text{eff}}(\mathbf{r}) = \delta v_{\text{ext}}(\mathbf{r}) + \delta v_{\text{scr}}(\mathbf{r}) = \delta v_{\text{ext}}(\mathbf{r}) + \int d^3r' I(\mathbf{r}, \mathbf{r}') \delta n(\mathbf{r}')$$

$$I(\mathbf{r}, \mathbf{r}') \equiv \frac{\delta v_{\text{scr}}(\mathbf{r})}{\delta n(\mathbf{r}')} = \frac{\delta v_{\text{H}}(\mathbf{r})}{\delta n(\mathbf{r}')} + \frac{\delta v_{\text{XC}}(\mathbf{r})}{\delta n(\mathbf{r}')} = \frac{2}{|\mathbf{r} - \mathbf{r}'|} + \frac{\delta^2 E_{XC}}{\delta n(\mathbf{r}) \delta n(\mathbf{r}')} \,. \tag{28}$$

This induces a first-order variation of the single-particle wavefunctions

$$\delta \psi_i(\mathbf{r}) = \sum_{j(\neq i)} \frac{\langle j | \delta v_{\text{eff}} | i \rangle}{\epsilon_i - \epsilon_j} \psi_j(\mathbf{r}) \,. \tag{29}$$

Using a similar expression for $\delta\psi_i^*(\mathbf{r})$ gives

$$
\begin{aligned}
\delta n(\mathbf{r}) &= \sum_i f_i[\psi_i^*(\mathbf{r})\delta\psi_i(\mathbf{r}) + \delta\psi_i^*(\mathbf{r})\psi_i(\mathbf{r})] \\
&= \sum_{i\neq j} \frac{f_i - f_j}{\epsilon_i - \epsilon_j}\langle j|\delta v_{\text{eff}}|i\rangle \psi_i^*(\mathbf{r})\psi_j(\mathbf{r})\,.
\end{aligned}
\tag{30}
$$

Eqs. (28) and (30) must be solved self-consistently to obtain the first-order variation of the density. To proceed, one can write the linear relationship (30) between δn and δv_{eff} more explicitly

$$
\delta n(\mathbf{r}) = \int d^3r'\chi_0(\mathbf{r},\mathbf{r}')\delta v_{\text{eff}}(\mathbf{r}')
\tag{31}
$$

$$
\chi_0(\mathbf{r},\mathbf{r}') = \sum_{i\neq j} \frac{f_i - f_j}{\epsilon_i - \epsilon_j}\psi_i^*(\mathbf{r})\psi_j(\mathbf{r})\psi_j^*(\mathbf{r}')\psi_i(\mathbf{r}')\,.
\tag{32}
$$

Here, χ_0 represents the charge susceptibility of the non-interacting Kohn-Sham system. It is expressed solely by ground-state quantities [24]. In the case of a periodic system, this is just the well-known Adler-Wiser form [25, 26]. Although obtained by perturbation theory, Eq. (32) is exact because the Kohn-Sham equations describe non-interacting electrons.
In combination with Eq. (28) this leads to

$$
\delta v_{\text{eff}} = \delta v_{\text{ext}} + I\chi_0\delta v_{\text{eff}}\,,
\tag{33}
$$

which can be solved for δv_{eff}

$$
\delta v_{\text{eff}} = [1 - I\chi_0]^{-1}\delta v_{\text{ext}} = \epsilon^{-1}\delta v_{\text{ext}}\,,
\tag{34}
$$

where $\epsilon = 1 - I\chi_0$ denotes the static dielectric matrix and describes the screening of the "bare" perturbation from the external potential.
The problem is now reduced to a calculation of ϵ^{-1}. Historically this was the first route to be explored [27, 28]. Direct application of these equations, however, has several practical disadvantages. It requires an inversion of the matrix $\epsilon(\mathbf{r},\mathbf{r}')$, which for periodic systems is most conveniently done in Fourier space. This inversion turns out to be the bottleneck of this scheme, as a proper convergence often requires a large number of Fourier components. Attempts to perform this inversion in direct space using a Wannier representation did not lead to significant improvements [29]. In the calculation of χ_0 in Eq. (32), unoccupied orbitals do enter, which are not available for bandstructure methods employing minimal basis sets (e.g. LMTO).

2.2.3 Modern formulation: Density functional perturbation theory

An important progress has been achieved by a new formulation of the linear-response approach that avoids some of the aforementioned problems of the dielectric matrix approach. It is called density functional perturbation theory (DFPT) and has been proposed independently by Zein *et al.* [30–32] and Baroni *et al.* [33, 34]. A concise description can be found in [35]. We will give a short outline for the case of a non-metallic system.

The expression (30) for the first-order density variation contains a double sum over electronic states. The prefactor $(f_i - f_j)/(\epsilon_i - \epsilon_j)$ restricts it to combinations where one state comes from the valence space and the other from the conduction space. Using time-reversal symmetry, this can be rewritten as

$$\delta n(\mathbf{r}) = 2 \sum_{vc} \frac{1}{\epsilon_v - \epsilon_c} \langle c|\delta v_{\text{eff}}|v\rangle \psi_v^*(\mathbf{r})\psi_c(\mathbf{r}) \,. \tag{35}$$

To avoid summation over the conduction states, one rewrites

$$\delta n(\mathbf{r}) = 2 \sum_v \psi_v^*(\mathbf{r})\Delta_v(\mathbf{r}) \tag{36}$$

with

$$|\Delta_v\rangle = \sum_c \frac{1}{\epsilon_v - \epsilon_c} |c\rangle\langle c|\delta v_{\text{eff}}|v\rangle \,. \tag{37}$$

This quantity fulfills the following linear equation:

$$(H - \epsilon_v)|\Delta_v\rangle = -\sum_c |c\rangle\langle c|\delta v_{\text{eff}}|v\rangle = -P_c \delta v_{\text{eff}}|v\rangle = (P_v - 1)\delta v_{\text{eff}}|v\rangle \,. \tag{38}$$

Here $P_c = \sum_c |c\rangle\langle c|$ denotes the projector onto the conduction space, and $P_v = 1 - P_c$ is the projector onto the valence space. By this reformulation, only valence-state quantities enter the equation for Δ_v, and one avoids an expensive summation over conduction states.

2.2.4   Beyond linear response: $(2n + 1)$ theorem

As shown above, the first derivative of the energy depends solely on the unperturbed ground-state density, while second-order derivatives require knowledge of the density and its first-order derivatives. Both results are special cases of the so-called $(2n+1)$ theorem, which states that all derivatives of the total energy up to $(2n + 1)$-th order with respect to the adiabatic perturbation can be calculated from the knowledge of all derivatives of the Kohn-Sham eigenstates and density up to n-th order. In the framework of density-functional theory this theorem also holds for nonlocal external potentials and is thus applicable within pseudopotential methods. The proof given by Gonze *et al.* [36–38] essentially rests on the variational property of the energy functional.

As a corollary of this theorem, harmonic as well as third-order anharmonic force constants merely require calculation of the linear variations of the Kohn-Sham eigenstates and the density. Both are accessible by linear-response calculations.

2.3   Phonons in periodic lattices

Here we discuss the details of the calculations of the interatomic force constants within the density functional perturbation approach. To this end, we consider periodic displacements of the ions from their equilibrium positions, $\mathbf{R}_{l\kappa} = \mathbf{R}_{l\kappa}^0 + \mathbf{u}_{l\kappa}$, of the form

$$u_{l\kappa\alpha} = d_{\kappa\alpha}e^{i\mathbf{q}\mathbf{R}_{l\kappa}^0} + d_{\kappa\alpha}^* e^{-i\mathbf{q}\mathbf{R}_{l\kappa}^0} \,, \tag{39}$$

where l denotes the unit cell, κ specifies the ion inside a unit cell, and α indicates Cartesian coordinates. The complex amplitudes $d_{\kappa\alpha}$ allow us to vary the relative phase of the displacement. It is convenient to denote the corresponding derivatives by $\delta^{\mathbf{q}}_{\kappa\alpha} \equiv \frac{\partial}{\partial d_{\kappa\alpha}}$ and $\delta^{-\mathbf{q}}_{\kappa'\beta} \equiv \frac{\partial}{\partial d^*_{\kappa\alpha}}$. The electronic contribution to the dynamical matrix can be then written as a mixed derivative

$$D_{\kappa\alpha\kappa'\beta}(\mathbf{q}) = \left. \frac{1}{\sqrt{M_\kappa M_{\kappa'}}} \delta^{\mathbf{q}}_{\kappa\alpha}\delta^{-\mathbf{q}}_{\kappa'\beta} E \right|_{\mathbf{u}=0}. \tag{40}$$

Usually, the external potential is expressed as a superposition of atomic potentials v_κ centered at the instantaneous positions of the ions

$$v_{\text{ext}}(\mathbf{r}) = \sum_{l\kappa} v_\kappa(\mathbf{r} - \mathbf{R}_{l\kappa}). \tag{41}$$

Its first-order variation, evaluated at the equilibrium positions, is given by

$$\begin{aligned}
\delta^{\mathbf{q}}_{\kappa\alpha} v_{\text{ext}}(\mathbf{r}) &= -\sum_l \nabla^{\mathbf{r}}_\alpha v_\kappa(\mathbf{r} - \mathbf{R}^0_{l\kappa}) e^{i\mathbf{q}\mathbf{R}^0_{l\kappa}} \\
&= -e^{i\mathbf{q}\mathbf{r}} \sum_l e^{i\mathbf{q}(\mathbf{R}^0_{l\kappa}-\mathbf{r})} \nabla^{\mathbf{r}}_\alpha v_\kappa(\mathbf{r} - \mathbf{R}^0_{l\kappa}).
\end{aligned} \tag{42}$$

The quantity defined by the lattice sum has the periodicity of the original lattice. Thus the derivative $\delta^{\mathbf{q}}_{\kappa\alpha}$ can be considered to carry a momentum $\mathbf{q}$.

When using a Bloch representation for the electronic eigenstates, the variation of the effective potential, $\delta^{\mathbf{q}}_{\kappa\alpha}v_{\text{eff}}$, connects states of momentum $\mathbf{k}$ with those of momentum $\mathbf{k} + \mathbf{q}$. The Fourier transform of the first order density variation takes the form

$$\delta^{\mathbf{q}}_{\kappa\alpha} n(\mathbf{q} + \mathbf{G}) = -\frac{4}{V} \sum_{\mathbf{k}v} \langle \mathbf{k}v | e^{-i(\mathbf{q}+\mathbf{G})\mathbf{r}} | \Delta^{\mathbf{q}}_{\kappa\alpha}(\mathbf{k}v) \rangle, \tag{43}$$

where V denotes the crystal volume. The quantity appearing on the right hand side is closely related to the first-order variation of the valence state $|\mathbf{k}v\rangle$ and is defined by (see Eq. (37))

$$|\Delta^{\mathbf{q}}_{\kappa\alpha}(\mathbf{k}v)\rangle = \sum_c \frac{|\mathbf{k}+\mathbf{q}c\rangle\langle\mathbf{k}+\mathbf{q}c|\delta^{\mathbf{q}}_{\kappa\alpha}v_{\text{eff}}|\mathbf{k}v\rangle}{\epsilon_c(\mathbf{k}+\mathbf{q}) - \epsilon_v(\mathbf{k})}. \tag{44}$$

It is obtained by solving the inhomogeneous linear equations (see Eq. (38))

$$(H^{\mathbf{k}+\mathbf{q}}_{KS} - \epsilon_v(\mathbf{k}))|\Delta^{\mathbf{q}}_{\kappa\alpha}(\mathbf{k}v)\rangle = (P^{\mathbf{k}+\mathbf{q}}_v - 1)\,\delta^{\mathbf{q}}_{\kappa\alpha}v_{\text{eff}}|\mathbf{k}v\rangle. \tag{45}$$

Eqs. (43) and (45) together with (28) constitute a set of equations that is solved self-consistently for a fixed $\mathbf{q}$ to obtain $\delta^{\mathbf{q}}_{\kappa\alpha}n$. As a by-product, $\delta^{\mathbf{q}}_{\kappa\alpha}v_{\text{eff}}$ is also calculated.

The electronic contribution to the dynamical matrix takes the form

$$\delta^{\mathbf{q}}_{\kappa\alpha}\delta^{-\mathbf{q}}_{\kappa'\beta}E = \sum_{\mathbf{G}} \left[\delta^{\mathbf{q}}_{\kappa\alpha}n(\mathbf{G}+\mathbf{q})\delta^{-\mathbf{q}}_{\kappa'\beta}v_{\text{ext}}(\mathbf{G}+\mathbf{q}) + \delta^{\mathbf{q}}_{\kappa\alpha}\delta^{-\mathbf{q}}_{\kappa'\beta}v_{\text{ext}}(\mathbf{G}) \right]. \tag{46}$$

Typically, first principles calculations along these lines are performed on a grid of $\mathbf{q}$-points that form a regular lattice and span the whole Brillouin zone. Discrete Fourier transforms are then applied to interpolate dynamical matrices on arbitrary points in between.

2.3.1   Technical aspects and extensions

The above derivation sketched the main ideas behind the perturbative approach. Practical implementations in existing band structure techniques require a variety of extensions and generalizations, which will be briefly discussed here.

Metals: Originally, the scheme was formulated for non-metallic systems and first applied in the framework of the plane-wave pseudopotential method. An extension to metallic systems has been derived by de Gironcoli, which contains essentially technical modifications related to the appearance of fractional occupation numbers for electronic states with energies close to the Fermi energy [39].

Non-local potentials: The above derivation assumed a local external potential. Modern pseudopotential approaches typically use also non-local forms, for which the above derivation is not strictly valid. It can be modified to include these forms, with the caveat that the dynamical matrix (46) cannot be expressed solely in terms of the density variation anymore but explicitly involves first-order variations of the wavefunctions, too.

Basis-set corrections: In many implementations, the electronic states are expanded in terms of a basis set. If the basis functions do not depend on the ionic positions, as is true of plane waves, the formulation given above is essentially unchanged. However, if the basis set depends explicitly on the position of the ions, it gives rise to additional contributions related to the change of the basis functions under an ionic displacement. These basis set corrections are known as Pulay corrections in the context of force calculations. Similar correction terms occur for methods based on ultrasoft pseudopotentials, as their construction requires the introduction of auxilliary charges centered at ionic sites.

Spin polarization: Extension to spin-polarized DFT is straightforward. The two spin sectors can be treated independently in the perturbation calculation, because the perturbation potential $\delta^{\mathbf{q}} v$ connects states of equal spins only. The dynamical matrix is then given as a sum of contributions from each spin.

Relativistic corrections: Extensions of the semi-relativistic framework, where spin-orbit coupling is neglected, have recently been worked out in the context of pseudopotentials [40, 41]. Here spin-orbit coupling can be easily incorporated by an additive term in the pseudopotential $v_{\text{ext}} \rightarrow v^{SR} + v^{SOC}$. It depends on the ion positions and gives rise to additional terms in δv_{ext} which entangle spatial and spin degrees of freedom.

3   Electron phonon coupling

3.1   Density functional perturbation approach to electron phonon vertex

3.1.1   Form of electron-phonon vertex

In the previous section, we have shown how the dynamics of the ions can be calculated quantitatively within the DFT approach. This was done on the basis of the adiabatic approximation, where the electronic subsystem entered the ionic equation-of-motion via a static screening term

only. Now we go one step further and consider the effect of a dynamical coupling between the electronic and phononic subsystems. Here, only the main ideas to derive the basic form of the electron-phonon vertex are sketched. A more elaborate discussion can be found in the book of Grimvall [42].

Let us consider again the general Hamiltonian of a solid given in Eq. (1) and look at the matrix element

$$\langle n\alpha|\mathcal{H}|n'\alpha'\rangle\,,\tag{47}$$

where a state $|n\alpha\rangle$ denotes the product of separate electronic and phononic wavefunctions. In the adiabatic approximation, only diagonal elements $n = n'$ and $\alpha = \alpha'$ are present. Non-vanishing off-diagonal elements come from the non-adiabatic terms ΔH in Eq. (6). For the most important one, $\Delta H^{(1)}$, one obtains

$$\langle n\alpha|\Delta H^{(1)}|n'\alpha'\rangle = \int \chi_\alpha^*(\psi_n^*\nabla_{\mathbf{R}}\psi_{n'})\cdot\nabla_{\mathbf{R}}\chi_{\alpha'}\,.\tag{48}$$

As before one assumes that all quantities are expanded around the equilibrium positions $\mathbf{R} = \mathbf{R}^0 + \mathbf{u}$ in a fast converging expansion in terms of u. To get an explicit expression, we describe the change in the electronic wavefunction by an effective potential $V(\underline{\mathbf{R}})$ due to small ionic displacements, giving

$$\int \psi_n^*\nabla_{\mathbf{R}}\psi_{n'} \propto \langle n|\nabla_{\mathbf{R}}V|n'\rangle\,,\tag{49}$$

where $|n\rangle$ and $|n'\rangle$ denote unperturbed electronic states. The remaining ionic matrix element $\int \chi_\alpha^*\nabla_{\mathbf{R}}\chi_{\alpha'}$ is proportional to the momentum operator, which depends linearly on the phonon creation and annihilation operators.

Thus the off-diagonal matrix elements in (47) describe the probability of emission or absorption of a phonon under a simultaneous excitation in the electronic subsystem. The electronic transition probabilities are determined by the first-order variation of the effective potential $V(\underline{\mathbf{R}})$ with respect to the ion coordinates as the perturbation operator.

3.1.2   Electron-phonon vertex in density functional perturbation theory

In the context of DFT, the electron-phonon coupling (EPC) matrix elements are defined as transition probabilities of Kohn-Sham states induced by a change in the potential due to a small ion displacement. If one would choose the electron-ion interaction potential, one obtains according to Eq. (42)

$$\langle \mathbf{k}+\mathbf{q}\nu'|\delta_{\kappa\alpha}^{\mathbf{q}}v_{\text{ext}}|\mathbf{k}\nu\rangle = -\langle \mathbf{k}+\mathbf{q}\nu'|e^{i\mathbf{q}\mathbf{r}}\sum_l e^{i\mathbf{q}(\mathbf{R}_{l\kappa}^0-\mathbf{r})}\nabla_\alpha^{\mathbf{r}}v_\kappa(\mathbf{r}-\mathbf{R}_{l\kappa}^0)|\mathbf{k}\nu\rangle\,.\tag{50}$$

It is convenient to switch to the normal-mode representation

$$g_{\mathbf{k}+\mathbf{q}\nu',\mathbf{k}\nu}^{(0)\mathbf{q}j} = \sum_{\kappa\alpha} A_{\kappa\alpha}^{\mathbf{q}j}\langle \mathbf{k}+\mathbf{q}\nu'|\delta_{\kappa\alpha}^{\mathbf{q}}v_{\text{ext}}|\mathbf{k}\nu\rangle\,,\tag{51}$$

where $\mathbf{q}j$ denotes the normal modes with momentum $\mathbf{q}$ and mode index j, and the coefficients $A_{\kappa\alpha}^{\mathbf{q}j}$ are defined in (16). This expression describes a rigid shift of the ionic potential, and
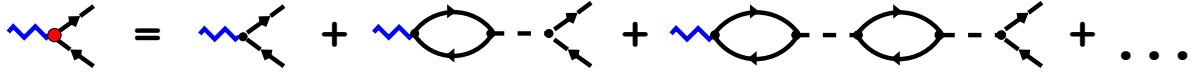
Fig. 1: *Diagrammatic representation of the screened electron-phonon vertex within the DFT framework. Blue zigzag lines represent phonons, black lines electron propagators, and the dashed lines the effective electron-electron interation.*

constitutes the so-called *bare* electron-phonon coupling matrix elements. Such a rigid-ion approximation is only justified in cases where all electrons are tightly bound to the ions as in an ionic crystal. For metals, in particular, this approximation typically fails, because it neglects the reaction of the electrons on the disturbance, which tend to screen the perturbation of the potential.

Within DFT the *screened* electron-phonon matrix elements are given by the variation of the effective potential

$$g^{\mathbf{q}\lambda}_{\mathbf{k}+\mathbf{q}\nu',\mathbf{k}\nu} = \sum_{\kappa\alpha} A^{\mathbf{q}j}_{\kappa\alpha} \langle \mathbf{k} + \mathbf{q}\nu' | \delta^{\mathbf{q}}_{\kappa\alpha} v_{\mathrm{eff}} | \mathbf{k}\nu \rangle \,. \tag{52}$$

It is instructive to look at it from a many-body perturbation perspective. Fig. 1 shows a diagrammatic representation of the screened vertex. The bare vertex is screened by virtual electron-hole excitations coupled via an effective interaction. From the relationship (34) between the external (bare) and effective (screened) perturbation, we can see that within the DFPT framework, the electron-hole bubble is represented by the charge-susceptibility of the non-interacting Kohn-Sham system (32). The effective interaction is given by the kernel I defined in Eq. (28) and incorporates both the Coulomb interaction and contributions from exchange and correlation.

We have seen in Sec. 2.3 that the first-order variation of the effective potential is calculated as a by-product in the DFPT self-consistent procedure. As the EPC matrix elements contain only this quantity and the unperturbed Kohn-Sham states, they can be calculated by a comparatively small numerical effort after a DFPT cycle is converged. They provide detailed microscopic information about how the coupling depends on the momenta of the electronic and phononic states as well as on the character of the electronic wavefunctions and the displacement pattern of the normal mode, respectively.

The spin dependence is incorporated in the EPC vertex in a straightforward way. In the semi-relativistic framework, when spin-orbit coupling is neglected, spin and spatial degrees-of-freedom are independent, and the perturbation due to the ion displacements does not flip the spin. As a consequence the EPC vertex is spin-diagonal. The EPC vertex in the presence of spin-orbit coupling has a more complex form. In the context of the pseudopotential method, it was shown that a second additive contribution to the perturbation operator appears, $\delta v_{\mathrm{eff}} \to \delta v^{SR}_{\mathrm{eff}} + \delta v^{SOC}$, which results in off-diagonal spin terms [43].

The EPC matrix elements are the essential ingredients for a numerical approach to a variety of physical properties. In the following I will discuss in some detail (i) renormalization of phonon properties, (ii) phonon-mediated pairing interaction and superconductivity, and (iii) self-energy effects for electronic states. Emphasis will be on how one can connect theoretical predictions with experimental observations to test the accuracy of the first principles EPC matrix elements,

(a) $\Pi(\omega)$ =

Fig. 2: *(a) Diagrammatic representation of the phonon self-energy up to second order in the electron-phonon vertex. Blue zigzag lines represent phonons, black lines electron propagators, and the dashed lines the effective electron-electron interaction. The leading contributions in the limit $\omega \to 0$ can be summed up with the help of the screened vertex introduced in Fig. 1. They are shown for (b) real part and (c) imaginary part of Π, respectively.*

which by themselves are not directly measurable.

In these applications one frequently encounters the problem that one needs EPC matrix elements on momentum grids, which are finer than the ones used in the DFPT cycle. Denser $\mathbf{k}$ grids can be applied in a straightforward way because the calculation of the EPC matrix elements is done separately from the DFPT part, so that only additional Kohn-Sham states need to be calculated. This is a numerically rather cheap procedure. In contrast, the DFPT calculation of $\delta^{\mathbf{q}}_{\kappa\alpha} v_{\text{eff}}$ is much more demanding. Therefore, matrix elements $g^{\mathbf{q}j}_{\mathbf{k}+\mathbf{q}\nu',\mathbf{k}\nu}$ for intermediate $\mathbf{q}$ are obtained by interpolation techniques. One way is to interpolate $\delta^{\mathbf{q}_i} v_{\text{eff}}$ given on a regular $\mathbf{q}_i$-grid and use exact Kohn-Sham states to evaluate the matrix elements. An alternative route is to use electron and phonon Wannier functions to represent the EPC matrix elements and utilize their spatial localization to interpolate them on very fine momentum grids [44, 45].

3.2   Phonon self-energy and linewidth

On the level of DFPT in the harmonic approximation, phonons are elementary excitations of the lattice, which do not interact and therefore have infinite lifetime. The interaction with electrons results in renormalized quasiparticle properties expressed by the phonon self-energy Π. The renormalized phonon Greens function is obtained from the bare Greens function $D_{0,\mathbf{q}j}(\omega) = 1/(\omega - \omega_{\mathbf{q}j}) - 1/(\omega + \omega_{\mathbf{q}j})$ via the Dyson equation $D^{-1} = D_0^{-1} - \Pi$ as

$$D_{\mathbf{q}j}(\omega) = \frac{2\omega_{\mathbf{q}j}}{\omega^2 - \omega_{\mathbf{q}j}^2 - 2\omega_{\mathbf{q}j}\Pi_{\mathbf{q}j}(\omega)} . \tag{53}$$

For not too large self-energies, the renormalization of the phonons leads to (i) a broadening of the quasiparticle peak of the spectral function, i.e. a finite linewidth, which is proportional to the inverse lifetime, and (ii) to a shift of the peak position. The linewidth is connected to $\text{Im}\Pi$, and the peak shift to $\text{Re}\Pi$.

In the following, we briefly sketch the approach to the phonon renormalization in the DFPT framework. It basically focuses on the lowest-order corrections beyond the adiabatic approximation. The starting point is a diagrammatic representation of the self-energy contributions coming from second-order EPC as sketched in Fig. 2(a). In general, the electron-hole bubble depends on the frequency ω and varies on the scale of electronic energies. These are usually much larger than typical phonon frequencies relevant for the renormalization. Therefore, to lowest order, one can take the static limit $\omega = 0$, and the series of diagrams can be summed up with the help of the screened vertex introduced above in Fig. 2(b). This gives a contribution to $\mathrm{Re}\Pi$ only, which has the form

$$\mathrm{Re}\Pi_{\mathbf{q}j}(0) = \frac{1}{N_k} \sum_{\mathbf{k}\nu\nu'} g^{\mathbf{q}j}_{\mathbf{k}+\mathbf{q}\nu',\mathbf{k}\nu} \left(g^{(0)\mathbf{q}j}_{\mathbf{k}+\mathbf{q}\nu'\mathbf{k}\nu}\right)^* \frac{f(\epsilon_{\mathbf{k}\nu}) - f(\epsilon_{\mathbf{k}+\mathbf{q}\nu'})}{\epsilon_{\mathbf{k}\nu} - \epsilon_{\mathbf{k}+\mathbf{q}\nu'}}. \tag{54}$$

Here $f(\epsilon) = (1 + e^{(\epsilon-\mu)/k_BT})^{-1}$ denotes the Fermi distribution function. Eq. (54) involves both the screened and bare vertices due to fact that the screening enters in a symmetric way, and using the screened vertex on both sides would result in a double counting of the diagrams containing the dashed lines.

It is now instructive to see that this static renormalization is already included in the DFPT procedure. This can be seen by using the definitions of the screened and bare vertices

$$\begin{aligned}
\mathrm{Re}\Pi_{\mathbf{q}j}(0) &= \frac{1}{N_k} \sum_{\mathbf{k}\nu\nu'} g^{\mathbf{q}j}_{\mathbf{k}+\mathbf{q}\nu',\mathbf{k}\nu} \left(g^{(0)\mathbf{q}j}_{\mathbf{k}+\mathbf{q}\nu'\mathbf{k}\nu}\right)^* \frac{f(\epsilon_{\mathbf{k}\nu}) - f(\epsilon_{\mathbf{k}+\mathbf{q}\nu'})}{\epsilon_{\mathbf{k}\nu} - \epsilon_{\mathbf{k}+\mathbf{q}\nu'}} \\
&= \frac{1}{N_k} \sum_{\mathbf{k}\nu\nu'} \sum_{\kappa\alpha\kappa'\beta} A^{\mathbf{q}j}_{\kappa\alpha} A^{-\mathbf{q}j}_{\kappa'\beta} \langle \mathbf{k}+\mathbf{q}\nu' | \delta^{\mathbf{q}}_{\kappa\alpha} v_{\mathrm{eff}} | \mathbf{k}\nu \rangle \langle \mathbf{k}\nu | \delta^{-\mathbf{q}}_{\kappa'\beta} v_{\mathrm{ext}} | \mathbf{k}+\mathbf{q}\nu' \rangle \\
&\quad \times \frac{f(\epsilon_{\mathbf{k}\nu}) - f(\epsilon_{\mathbf{k}+\mathbf{q}\nu'})}{\epsilon_{\mathbf{k}\nu} - \epsilon_{\mathbf{k}+\mathbf{q}\nu'}} \\
&= \frac{1}{N_k} \sum_{\mathbf{k}\nu\nu'} \sum_{\kappa\alpha\kappa'\beta} A^{\mathbf{q}j}_{\kappa\alpha} A^{-\mathbf{q}j}_{\kappa'\beta} \int d^3r\, \delta^{\mathbf{q}}_{\kappa\alpha} n(\mathbf{r}) \delta^{-\mathbf{q}}_{\kappa'\beta} v_{\mathrm{ext}}(\mathbf{r}).
\end{aligned} \tag{55}$$

In the last step the linear-response expression (30) for the first-order variation of the electronic density was applied. Comparison with Eq. (46) shows that this term corresponds to the first contribution to the dynamical matrix which comes from the variation of the density. Thus this renormalization is already taken into account on the level of DFPT.

The situation is different for $\mathrm{Im}\Pi$. This is a true non-adiabatic property, and one has to go beyond the static approximation. The dominant contribution in the limit $\omega \to 0$ is obtained by replacing in each term of the series in Fig. 2(a) one electron-hole bubble by its imaginary part and taking the static limit for all others. Then again, the series can be summed up, but now both vertices in the diagram are screened (Fig. 2(c)). This leads to the following expression for the linewidth (half-width at half maximum)

$$\begin{aligned}
\gamma_{\mathbf{q}j} &= -2\,\mathrm{Im}\Pi_{\mathbf{q}j}(\omega_{\mathbf{q}j}) \\
&= 2\pi \frac{1}{N_k} \sum_{\mathbf{k}\nu\nu'} \left| g^{\mathbf{q}j}_{\mathbf{k}+\mathbf{q}\nu',\mathbf{k}\nu} \right|^2 \left(f(\epsilon_{\mathbf{k}\nu}) - f(\epsilon_{\mathbf{k}+\mathbf{q}\nu'})\right) \delta\left(\omega_{\mathbf{q}j} + (\epsilon_{\mathbf{k}\nu} - \epsilon_{\mathbf{k}+\mathbf{q}\nu'})\right). \tag{56}
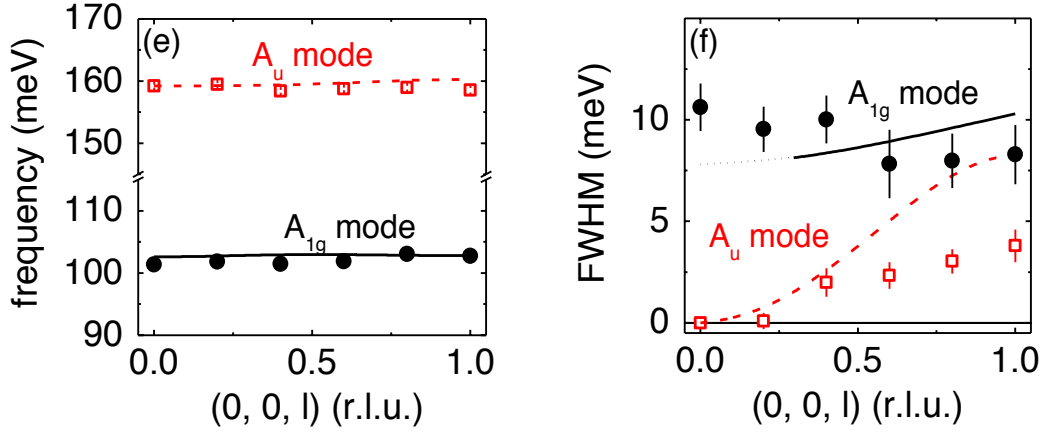\end{aligned}$$

Fig. 3: *Phonon dispersion (left panel) and linewidths (right panel) for two high-frequency branches of YNi$_2$B$_2$C along the [001] direction. Shown are inelastic neutron scattering results (symbols) together with first principles predictions (lines) [47].*

This expression contains the T-dependence via the Fermi distribution functions f. It can be further simplified as long as the electronic structure has no peculiarities on the scale of phonon energies. The δ-function forces the energy difference $\epsilon_{\mathbf{k}\nu} - \epsilon_{\mathbf{k}+\mathbf{q}\nu'}$ to be small, hence the difference of the Fermi distribution functions can be approximated with the help of its energy derivative $f' = df/d\epsilon$

$$f(\epsilon_{\mathbf{k}\nu}) - f(\epsilon_{\mathbf{k}+\mathbf{q}\nu'}) \approx f'(\epsilon_{\mathbf{k}\nu})(\epsilon_{\mathbf{k}\nu} - \epsilon_{\mathbf{k}+\mathbf{q}\nu'}) \rightarrow -f'(\epsilon_{\mathbf{k}\nu})\omega_{\mathbf{q}j} \,. \tag{57}$$

Finally, the phonon frequency is neglected in the δ function.

At low temperatures, the energy derivative of the Fermi distribution function is strongly peaked at the Fermi energy. In the limit $T \rightarrow 0$, it can be replaced by $f'(\epsilon_{\mathbf{k}\nu}) \rightarrow -\delta(\epsilon_{\mathbf{k}\nu} - \epsilon_F)$. We finally arrive at an expression for the EPC-induced phonon linewidth valid in the limit $T \rightarrow 0$

$$\gamma_{\mathbf{q}j} = 2\pi\omega_{\mathbf{q}j} \frac{1}{N_k} \sum_{\mathbf{k}\nu\nu'} |g^{\mathbf{q}j}_{\mathbf{k}+\mathbf{q}\nu',\mathbf{k}\nu}|^2 \delta(\epsilon_{\mathbf{k}\nu} - \epsilon_F)\delta(\epsilon_{\mathbf{k}+\mathbf{q}\nu'} - \epsilon_F) \,. \tag{58}$$

It contains only quantities that are available within the DFPT approach to the EPC. The derivation of (58) was first given by Allen [46]. This form of the linewidth is most often used in first-principles calculations. One must, however, be aware of the approximations underlying its derivation. It is only valid in the limit $T \rightarrow 0$ and also breaks down in the limit $\mathbf{q} \rightarrow 0$ for metals because intraband scattering events involve arbitrarily small energy differences $\epsilon_{\mathbf{k}\nu} - \epsilon_{\mathbf{k}+\mathbf{q},\nu}$, and the phonon frequency cannot be neglected anymore.

Phonon linewidths can be measured by, e.g., inelastic neutron or x-ray scattering experiments. However, when comparing theory and experiment, one should keep in mind that the above formula only represents the contribution to the linewidth coming from EPC. Experimentally, one needs to separate it from other possible contributions to the linewidth, most importantly those related to anharmonic decay processes, which often is not easy to achieve.

An example is shown for two high-frequency modes of the superconductor YNi$_2$B$_2$C in Fig. 3. Measurements were done at low T, where anharmonic contributions are supposed to play a

minor role. The calculations do predict the size and momentum dependence of the linewidths reasonably well, demonstrating that even for compounds with rather complex lattice structure these calculations are reliable.

As we will see in the discussion of superconductivity given below, the same expression (58) enters the pairing properties. As such Eq. (58) provides a link between the pairing strength of a phonon mode and the linewidth, the latter being an experimentally accessible quantity.

As discussed in Sec. 3.1, the concept of electron-phonon coupling goes beyond the adiabatic approximation, and we leave the firm base of DFT. The above derivation showed, however, that to a first approximation the phonon linewidth can still be calculated within the DFPT scheme. To include further non-adiabatic corrections as for, e.g., the frequency renormalization, a more general framework like the time-dependent DFT is required. Such a generalization was outlined recently by Saitta *et al.* [48].

3.3   Phonon mediated pairing interaction and superconductivity

Superconductivity is a macroscopic quantum phenomenon of the electron system. Its origin lies in an instability of the Fermi liquid state and leads to a new ground state of correlated paired electrons (Cooper pairs). In their seminal paper, Bardeen, Cooper, and Schrieffer (BCS) [49] have shown that this state is stabilized when there is a small attractive interaction among two electrons. Such an attractive interaction is always provided by the electron-phonon coupling, which thus represents a natural source for pairing in any metal. EPC is known to be the pairing mechanism in most superconductors, which are commonly termed classical superconductors to distinguish them from more exotic materials where other types of pairing mechanism are suspected.

The BCS theory treated the EPC only in a simplified form appropriate for the weak coupling limit. Soon after a more complete theory was worked out, applying many-body techniques (for a review see, e.g., Scalapino [50]) . The resulting Eliashberg theory [51] extends the framework of BCS into the strong coupling regime and allows a quantitative prediction of many properties of the superconducting state. An important property of the superconducting state is that the quasiparticle spectrum is gapped. The size of the gap plays the role of an order parameter. It is determined from a self-consistent solution of a set of equations which generalize the BCS gap equations. An important feature of these so-called Eliashberg gap equations is that only normal-state properties enter, which specify a particular material. These include details about the electronic structure and the phonon-mediated pairing interaction, quantities which are readily accessible within the first principles approach to EPC outlined above.

As the Eliashberg theory will be presented in detail in another lecture of this Autumn School, I will focus here on the procedure to calculate the effective electron-electron interaction. The physical process behind the phonon-mediated interaction is the exchange of a phonon between two electrons, shown schematically in Fig. 4. This translates into the so-called Eliashberg function

$$\alpha^2 F_{\mathbf{k}\nu,\mathbf{k}'\nu'}(\omega) = N(\epsilon_F) \frac{1}{N_q} \sum_{\mathbf{q}j} |g^{\mathbf{q}j}_{\mathbf{k}'\nu',\mathbf{k}\nu}|^2 \, \delta(\omega - \omega_{\mathbf{q}j}) \,. \tag{59}$$
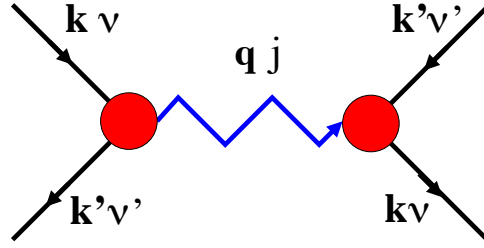
Fig. 4: *Diagrammatic representation of the effective electron-electron interaction mediated by the exchange of a phonon.*

Here $N(\epsilon_F)$ is the electronic density-of-states at the Fermi energy per spin. The sum extends over all phonon modes mediating the interaction, which also determine its frequency dependence. Both coupling vertices are represented by screened matrix elements, and its implicit momentum conservation restricts the sum to $\mathbf{q} = \mathbf{k}' - \mathbf{k}$. For the superconducting pairing, this interaction is most effective for electronic states with energies $|\epsilon_{\mathbf{k}\nu} - \epsilon_F| \leq \omega_{\text{phonon}}$. Thus, in practice one evaluates (59) only for states right at the Fermi surface (for an elaborate discussion of the underlying assumptions and approximations see [52]).

Most superconductors exhibit surprisingly isotropic superconducting gaps. The reason is that defects, which are always present in real materials, tend to wash out the momentum dependence of the interaction. In many cases, it is sufficient to consider the Fermi surface average leading to the isotropic Eliashberg function $\alpha^2 F(\omega) = \sum_{\mathbf{k}\nu, \mathbf{k}'\nu'} w_{\mathbf{k}\nu} w_{\mathbf{k}'\nu'} \alpha^2 F_{\mathbf{k}\nu, \mathbf{k}'\nu'}(\omega)$ with $w_{\mathbf{k}\nu} = \delta(\epsilon_{\mathbf{k}\nu} - \epsilon_F)/N(\epsilon_F)$. Taking momentum conservation into account, this is typically cast into the form

$$\alpha^2 F(\omega) = \frac{1}{N(\epsilon_F)} \frac{1}{N_q} \sum_{\mathbf{q}j, \mathbf{k}\nu\nu'} |g_{\mathbf{k}+\mathbf{q}\nu', \mathbf{k}\nu}^{\mathbf{q}j}|^2 \delta(\omega - \omega_{\mathbf{q}j}) \delta(\epsilon_{\mathbf{k}\nu} - \epsilon_F) \delta(\epsilon_{\mathbf{k}+\mathbf{q}\nu'} - \epsilon_F) . \tag{60}$$

Within Eliashberg theory, important characteristics like the superconducting transition temperature often depend on integrated quantities only. One such quantity is the isotropic coupling constant defined by

$$\lambda = 2 \int d\omega \, \frac{\alpha^2 F(\omega)}{\omega} , \tag{61}$$

which is the dimensionless measure of the average strength of the coupling. Commonly, values larger than 1 are characterized as strong coupling. The factor $1/\omega$ in the integral indicates that low-energy modes are generally more effective than high-energy modes in mediating the pairing.

At this stage it is useful to make a connection to the expression for the phonon linewidth derived in the limit $T \to 0$. Using Eq. (58), the isotropic Eliashberg function can be written as

$$\alpha^2 F(\omega) = \frac{1}{2\pi N(\epsilon_F)} \frac{1}{N_q} \sum_{\mathbf{q}j} \frac{\gamma_{\mathbf{q}j}}{\omega_{\mathbf{q}j}} \delta(\omega - \omega_{\mathbf{q}j}) \tag{62}$$

and the isotropic coupling constant as

$$\lambda = \frac{1}{\pi N(\epsilon_F)} \frac{1}{N_q} \sum_{\mathbf{q}j} \frac{\gamma_{\mathbf{q}j}}{\omega_{\mathbf{q}j}^2} . \tag{63}$$

The dimensionless prefactor $\gamma_{\mathbf{q}j}/\omega_{\mathbf{q}j}$ in (62) can be interpreted as a measure of the coupling due to an individual phonon mode. The Eliashberg function is then given as a sum over all phonon branches and averaged over phonon momentum.

Commonly, DFPT based calculations of the Eliashberg function are done by first calculating $\gamma_{\mathbf{q}j}$ and then performing the sum over the phonon spectrum. The appearance of a product of δ-functions in the expression (58), however, requires a careful numerical approach. Usually the δ-functions are replaced by smoother functions like Gaussians, but to reach convergence the $\mathbf{k}$-summation has to be carried out on meshes which are denser than the one used for the calculation of the phonon properties.

The strong-coupling superconductor Pb illustrates this general approach well because the effects of EPC are especially pronounced and relativistic corrections are necessary for a satisfactory quantitative description. Fig. 5(a) shows the phonon dispersion along high-symmetry directions, comparing semi-relativistic (SR) results and those including the spin-orbit coupling (SOC) with data from inelastic neutron-scattering experiments. The experimental scale of phonon frequencies, and in particular the pronounced anomalous dips observed at various points along the dispersion curves are fingerprints of strong EPC. They are much better reproduced when SOC is included, which in addition improves the whole spectrum by lowering the frequencies as compared to the SR calculation. Phonon linewidths shown in Fig. 5(b) for the same branches exhibit a strong variation as a function of momentum. The values are generally larger for the SOC calculation, indicating that the matrix elements are enhanced significantly. This is reflected in an enhanced $\alpha^2 F$ shown in Fig. 5(c), which much better agrees with the Eliashberg function derived from tunneling spectroscopy experiments. The isotropic coupling constant λ is increased from 1.08 to 1.56 by SOC, which matches well the experimental value of 1.55. A closer look at the different contributions to λ reveals that about half of this increase originates in the softening of the spectrum (due to the factor $1/\omega$ in the expression for λ), while the other half comes from an increase of the coupling matrix elements. This example demonstrates that SOC can substantially modify the EPC [43].

Anisotropic superconducting states can be handled using the full momentum dependence of the Eliashberg function (59). This has been done rarely in the past, as the fully anisotropic gap equations are difficult to solve. A special class of anisotropic superconductors are multiband superconductors, which possess several Fermi surface sheets. The superconducting gap can vary among the different sheets but is approximately isotropic on a single sheet. In this case, a partially averaged pairing function is appropriate

$$\alpha^2 F_{\nu\nu'}(\omega) = \frac{1}{N(\epsilon_F)} \frac{1}{N_q} \sum_{\mathbf{q}j,\mathbf{k}} |g^{\mathbf{q}j}_{\mathbf{k}+\mathbf{q}\nu',\mathbf{k}\nu}|^2 \delta(\omega - \omega_{\mathbf{q}j}) \delta(\epsilon_{\mathbf{k}\nu} - \epsilon_F) \delta(\epsilon_{\mathbf{k}+\mathbf{q}\nu'} - \epsilon_F). \qquad (64)$$

The isotropic Eliashberg function is replaced by a matrix describing intraband and interband pairing contributions.

A textbook example of such a multiband superconductor is MgB_2. Here two types of electronic states are present at the Fermi level: σ and π states, which are derived mainly from the boron p states. Calculations of the band-resolved Eliashberg functions shown in Fig. 6 revealed that the
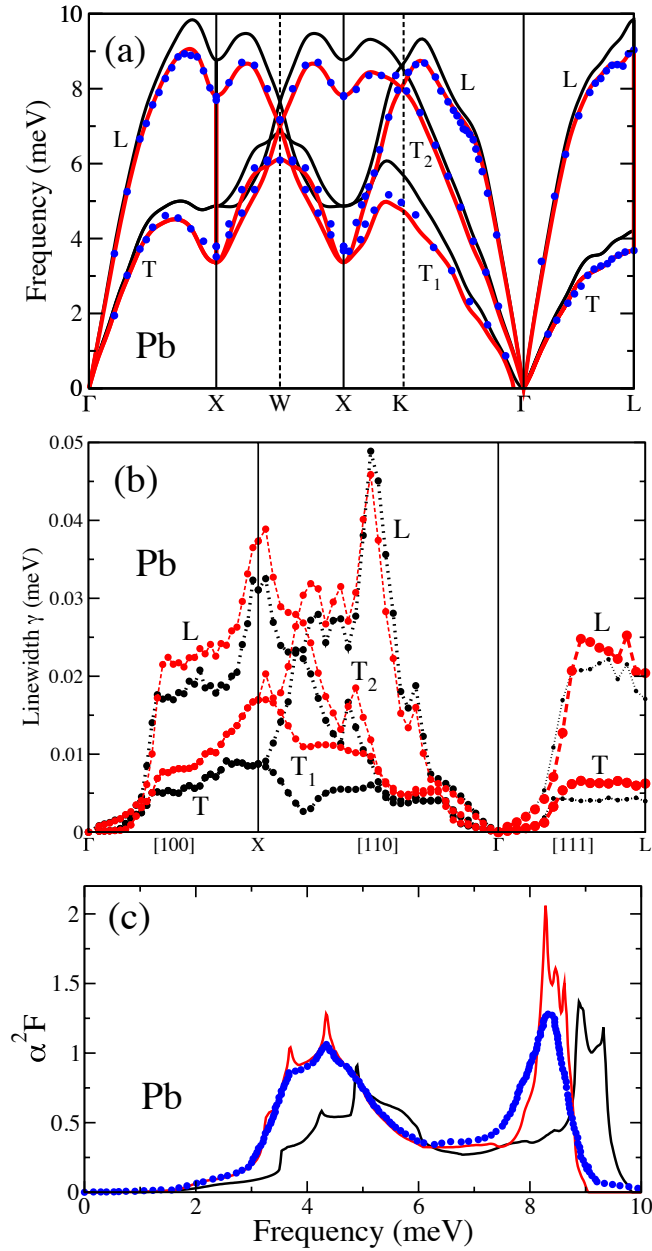
Fig. 5: *Phonon and electron-phonon coupling properties for the elemental superconductor Pb. Figures show (a) the phonon dispersion, (b) the mode-dependent linewidth, and (c) the Eliashberg function (c). Black lines indicate results of calculations without spin-orbit coupling, and red lines with spin-orbit coupling included. For comparison, blue symbols show experimental results for (a) phonon frequencies obtained from inelastic neutron scattering experiments [53] and (c) the Eliashberg function extracted from tunneling spectroscopy data [54].*

pairing interaction is predominantly driven by the intraband σ-σ contribution. It originates from a strong coupling to in-plane B vibrations which drive a large softening of branches connected to the E_{2g} modes (left panel in Fig. 6). This peculiar pairing interaction leads to a superconducting state with gaps of different magnitude for the σ and π Fermi surfaces whose signature could be found, e.g., in specific heat measurements. Tunneling spectroscopy gave strong support for the predicted multiband pairing spectrum [55], too.
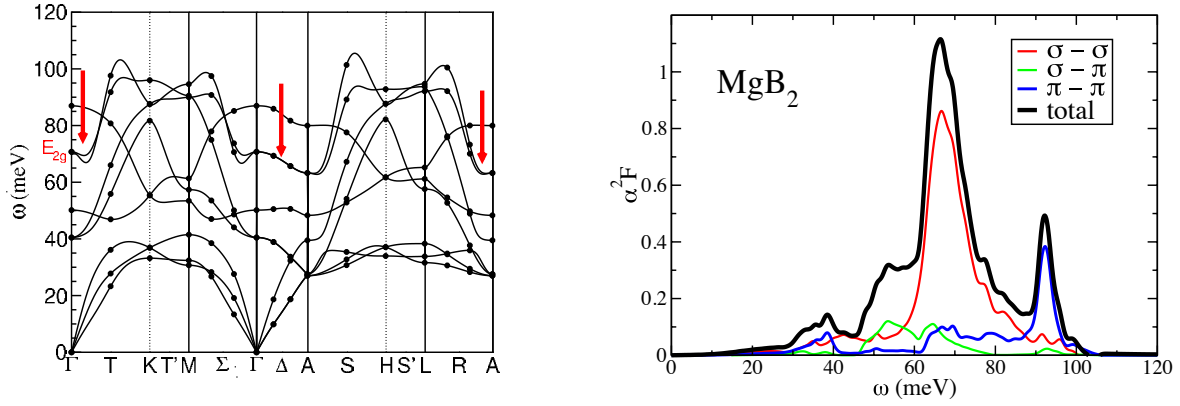
Fig. 6: *Left panel: Calculated phonon dispersion of the multiband superconductor MgB$_2$. The large frequency softening of the E_{2g}-related branches due to a very strong EPC is indicated by red arrows. Right panel: Calculated total and band-resolved Eliashberg functions of MgB$_2$ demonstrating that the dominant coupling originates from a large intraband σ-σ pairing interaction.*

3.4 Electron self-energy effects

Another important physical consequence of EPC is the renormalization of electronic quasiparticles. This has particularly profound consequences for metals, as it strongly modifies electronic states whose energy distance to the Fermi level is of the order of the phonon energies. Although this is a small energy compared to typical electronic scales, it significantly influences Fermi surface related properties like transport or thermodynamics.

Nowadays, there are a variety of experimental techniques that can probe the properties of electronic quasiparticles in fine detail. A well known example is angle-resolved photoemission spectroscopy (ARPES), which essentially measures the quasiparticle spectral function of occupied states, while unoccupied states can be accessed by, e.g., pump-probe experiments. Such studies provide information about the energy and momentum dependence of the renormalization due to EPC. As these techniques are rather surface sensitive, most applications were devoted to surface electronic states (for a recent review, see [56]).

The renormalization is described by the electron self-energy, which via the Dyson equation enters the renomalized electronic Green's function as

$$G(\mathbf{k}\nu, \epsilon) = \left(\epsilon - (\epsilon_{\mathbf{k}\nu} - \mu) - \Sigma(\mathbf{k}\nu, \epsilon)\right)^{-1}. \tag{65}$$

For not-too-large self-energies, the spectral function $A_{\mathbf{k}\nu}(\epsilon) = -\mathrm{Im}G(\mathbf{k}\nu, \epsilon + i\delta)$ possesses a well defined peak at a shifted quasiparticle energy determined by the real part of Σ

$$\bar{\epsilon}_{\mathbf{k}\nu} = \epsilon_{\mathbf{k}\nu} - \mathrm{Re}\Sigma(\mathbf{k}\nu, \bar{\epsilon}_{\mathbf{k}\nu}). \tag{66}$$

The quasiparticle acquires a finite lifetime leading to a linewidth (FWHM)

$$\Gamma_{\mathbf{k}\nu} = -2\mathrm{Im}\Sigma(\mathbf{k}\nu, \bar{\epsilon}_{\mathbf{k}\nu}) \tag{67}$$

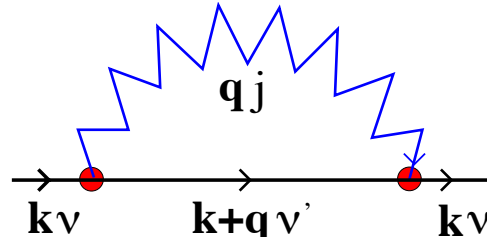that is determined by the imaginary part.

Fig. 7: *Diagrammatic representation of the lowest-order contribution to the electron self-energy from the electron-phonon coupling.*

The relevant lowest order diagram due to EPC is shown in Fig. 7. It describes a virtual exchange of a phonon. Note that in this case both coupling vertices are screened. This leads to the following expression

$$\Sigma(\mathbf{k}\nu, \epsilon) = \frac{1}{N_q} \sum_{\mathbf{q}j} \sum_{\nu'} \left|g^{\mathbf{q}j}_{\mathbf{k}+\mathbf{q}\nu',\mathbf{k}\nu}\right|^2 \left(\frac{b(\omega_{\mathbf{q}j}) + f(\epsilon_{\mathbf{k}+\mathbf{q}\nu'})}{\epsilon + \omega_{\mathbf{q}j} - \epsilon_{\mathbf{k}+\mathbf{q}\nu'} + i\delta} + \frac{b(\omega_{\mathbf{q}j}) + 1 - f(\epsilon_{\mathbf{k}+\mathbf{q}\nu'})}{\epsilon - \omega_{\mathbf{q}j} - \epsilon_{\mathbf{k}+\mathbf{q}\nu'} + i\delta} \right). \quad (68)$$

The T dependence now enters via both Fermi and Bose distribution functions, $f(\epsilon)$ and $b(\omega) = [e^{\omega/k_B T} - 1]^{-1}$, respectively.

From Eq. (68) one can readily derive the expression for the imaginary part. It is convenient to introduce two spectral functions which depend explicitly on the electronic state $(\mathbf{k}\nu)$

$$\alpha^2 F^{\pm}_{\mathbf{k}\nu}(\epsilon, \omega) = \frac{1}{N_q} \sum_{\mathbf{q}j} \delta(\omega - \omega_{\mathbf{q}j}) \sum_{\nu'} \left|g^{\mathbf{q}j}_{\mathbf{k}+\mathbf{q}\nu',\mathbf{k}\nu}\right|^2 \delta(\epsilon - \epsilon_{\mathbf{k}+\mathbf{q}\nu'} \pm \omega). \quad (69)$$

Then the imaginary part can be cast in the form

$$\mathrm{Im}\Sigma_{\mathbf{k}\nu}(\epsilon) = -\pi \int_0^\infty d\omega \left\{ \alpha^2 F^+_{\mathbf{k}\nu}(\epsilon, \omega)[b(\omega) + f(\omega + \epsilon)] + \alpha^2 F^-_{\mathbf{k}\nu}(\epsilon, \omega)[b(\omega) + f(\omega - \epsilon)] \right\}. \quad (70)$$

The appearance of δ-functions in (69) allows a straightforward numerical evaluation of Eq. (70). In contrast, a direct calculation of $\mathrm{Re}\Sigma(\mathbf{k}\nu, \epsilon)$ via Eq. (68) requires a summation over many intermediate electronic states, which converges slowly. Therefore, in practice, one obtains $\mathrm{Re}\Sigma$ by making use of the Kramers-Kronig relation

$$\mathrm{Re}\Sigma(\mathbf{k}\nu, \epsilon) = \frac{1}{\pi} \int d\epsilon' \frac{\mathrm{Im}\Sigma(\mathbf{k}\nu, \epsilon')}{\epsilon - \epsilon'}. \quad (71)$$

From (70) one readily obtains an expression for the EPC-induced quasiparticle linewidth

$$\Gamma_{\mathbf{k}\nu} = 2\pi \int_0^\infty d\omega \left\{ \alpha^2 F^+_{\mathbf{k}\nu}(\bar{\epsilon}_{\mathbf{k}\nu}, \omega)[b(\omega) + f(\omega + \bar{\epsilon}_{\mathbf{k}\nu})] + \alpha^2 F^-_{\mathbf{k}\nu}(\bar{\epsilon}_{\mathbf{k}\nu}, \omega)[b(\omega) + f(\omega - \bar{\epsilon}_{\mathbf{k}\nu})] \right\}. \quad (72)$$

The two terms in this expression represent two different scattering processes, which are sketched in Fig. 8. When a quasiparticle hole is created at the state $(\mathbf{k}\nu)$, electrons can scatter from states with higher or lower energies, respectively. To conserve the total energy, the first process is connected with the emission of a phonon and is described by $\alpha^2 F^-_{\mathbf{k}\nu}$. On the other hand, $\alpha^2 F^+_{\mathbf{k}\nu}$ describes the scattering of an electron from a lower-energy state with the simultaneous
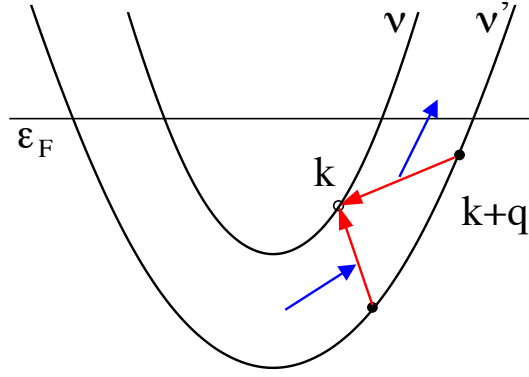
Fig. 8: *Illustration of the scattering processes contributing to the self-energy of a hole quasi-particle with momentum* **k** *and band index* ν. *Electrons (red lines) can scatter virtually from states with higher or lower energies under simultaneous emission or absorption of a phonon (blue lines), respectively.*

absorption of a phonon. A similar interpretation can be given if a quasiparticle is created at energies $\epsilon > \epsilon_F$.

While the emission and absorption spectra differ in principle, it is often found in practice that the differences are small. This is due to the fact that the electronic energy scale is typically much larger than the phonon energies. Therefore, emission or absorption of a phonon mainly changes the momentum of the electron, while the energy change is negligible. In this case the phonon energy in the δ-function of (69) can be dropped resulting in $\alpha^2 F_{\mathbf{k}\nu}^{\pm} \approx \alpha^2 F_{\mathbf{k}\nu}$, with the spectral function

$$\alpha^2 F_{\mathbf{k}\nu}(\epsilon, \omega) = \frac{1}{N_q} \sum_{\mathbf{q}j} \delta(\omega - \omega_{\mathbf{q}j}) \sum_{\nu'} \left| g_{\mathbf{k}+\mathbf{q}\nu', \mathbf{k}\nu}^{\mathbf{q}j} \right|^2 \delta(\epsilon - \epsilon_{\mathbf{k}+\mathbf{q}\nu'}) . \tag{73}$$

This so-called quasielastic approximation leads to the simplified expression of the linewidth

$$\Gamma_{\mathbf{k}\nu} = \pi \int_0^{\infty} d\omega \left\{ \alpha^2 F_{\mathbf{k}\nu}(\bar{\epsilon}_{\mathbf{k}\nu}, \omega)[2b(\omega) + f(\omega + \bar{\epsilon}_{\mathbf{k}\nu}) + f(\omega - \bar{\epsilon}_{\mathbf{k}\nu})] \right\} . \tag{74}$$

The coupling parameter is defined via

$$\lambda_{\mathbf{k}\nu} = 2 \int d\omega \, \frac{\alpha^2 F_{\mathbf{k}\nu}(\epsilon_{\mathbf{k}\nu}, \omega)}{\omega} . \tag{75}$$

This dimensionless quantity characterizes the interaction strength of a specific electronic state to the whole phonon spectrum, and depends both on the momentum and band character of the electronic state. Numerical evaluation of the sum in (73) requires typically rather dense **q**-meshes to reach convergence. To get the related matrix elements one resorts to interpolation techniques mentioned in Sec. 3.1.2.

The Eliashberg function discussed in Sec. 3.3 is related to this state-dependent spectral function via appropriate momentum averages at the Fermi energy. For the isotropic Eliashberg function the relation $\alpha^2 F(\omega) = \sum_{\mathbf{k}\nu} w_{\mathbf{k}\nu} \alpha^2 F_{\mathbf{k}\nu}(\epsilon_F, \omega)$ holds with weights $w_{\mathbf{k}\nu} = \delta(\epsilon_{\mathbf{k}\nu} - \epsilon_F)/N(\epsilon_F)$, and the isotropic coupling constant is given by $\lambda = \sum_{\mathbf{k}\nu} w_{\mathbf{k}\nu} \lambda_{\mathbf{k}\nu}$.
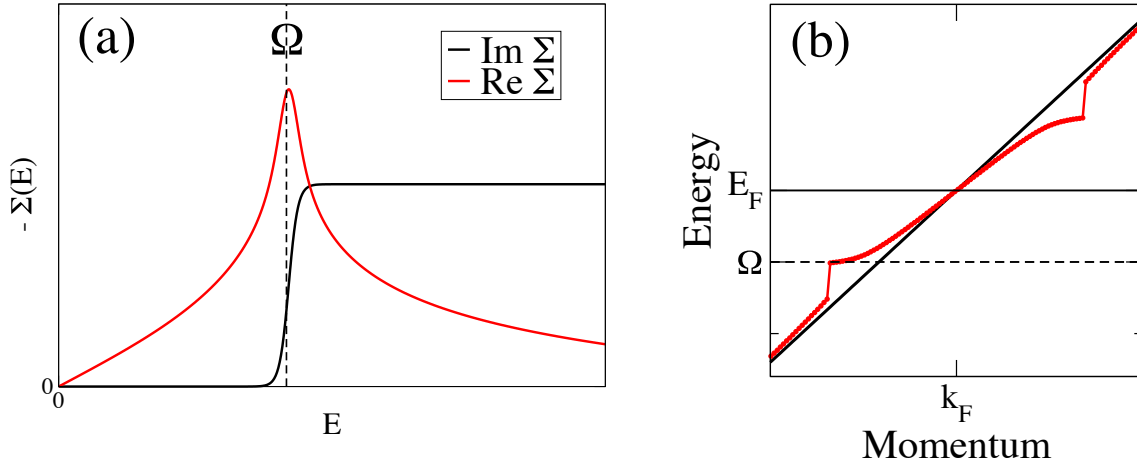
Fig. 9: *Illustration of the renormalization of an electronic band for a model coupling to an Einstein-type phonon branch with energy Ω. (a) Real and imaginary part of the electron self-energy. (b) Renormalized quasiparticle dispersion, showing a kink at the phonon frequency.*

Experimentally, the coupling strength of individual electronic states can be probed in two different ways. The first is related to the T-dependence of the linewidth. In Eq. (74), it is contained solely in the Bose and Fermi distribution functions. One can easily derive its behavior for the two limiting cases, $T \to 0$ and large T. For $T \to 0$, $n(\omega)$ vanishes and one obtains

$$\Gamma_{\mathbf{k}\nu} \to 2\pi \int_0^{\omega_{\max}} d\omega \, \alpha^2 F_{\mathbf{k}\nu}(\bar{\epsilon}_{\mathbf{k}\nu}, \omega) \,. \tag{76}$$

With increasing temperature, the linewidth increases for all energies. For temperatures larger than the maximum phonon frequency, this T-dependence becomes linear, and its slope is determined by the average coupling parameter defined above

$$\Gamma_{\mathbf{k}\nu} \approx 2\pi \lambda_{\mathbf{k}\nu} k_B T \,. \tag{77}$$

This relationship has been widely used to extract $\lambda_{\mathbf{k}\nu}$ from measurements of $\Gamma_{\mathbf{k}\nu}(T)$ for surface electronic states. The analysis is, however, complicated by the fact that the measured linewidth also contains contributions from other decay channels, most noticeably due to electron-electron interaction and due to elastic scattering at defects.

A second route to connecting theory and experiment are ARPES measurements of the spectral function of electronic bands close to the Fermi energy. They provide more direct information about the renormalization and the underlying self-energy. It is instructive to first look at a simple model where only a single dispersionless phonon branch is involved in the coupling, i.e. $\alpha^2 F_{\mathbf{k}\nu}(\omega)$ possesses one δ-type peak at the phonon frequency Ω (Einstein model). Fig. 9(a) shows the resulting self-energy for $T \to 0$. Its imaginary part exhibits a step at Ω because, for $\omega < \Omega$, no phonons are available to promote the scattering, while for $\omega > \Omega$ this scattering channel is opened. The real part of the self-energy exhibits a peak at the phonon frequency, which shows that the largest shifts of the quasiparticle peaks occur for electronic states with $\bar{\epsilon} - \epsilon_F \approx \Omega$. As a consequence, the renormalized dispersion shown in Fig. 9(b) exhibits a kink-like structure right at the phonon energy.
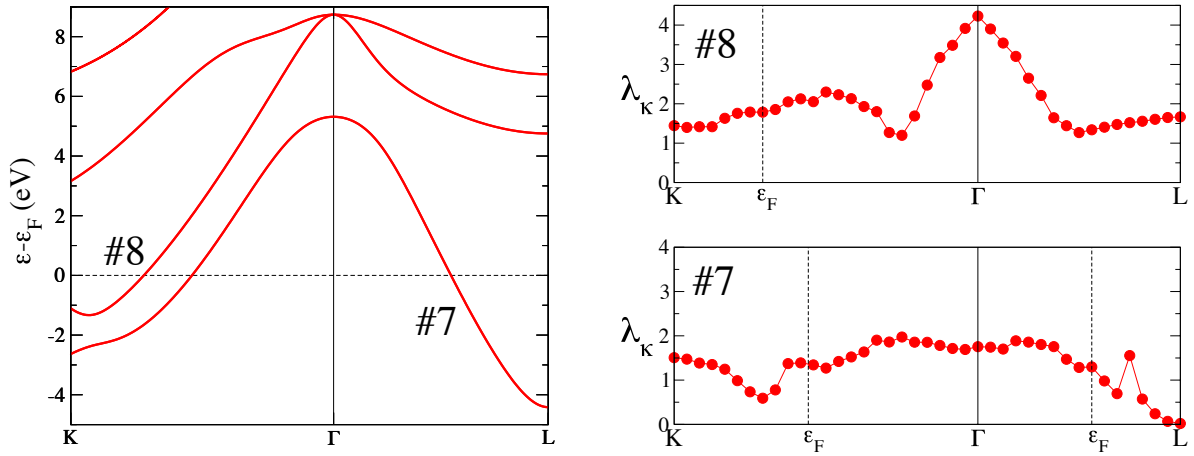
Fig. 10: *Electronic-state dependent coupling constants for Pb. Left panel: band structure along the high-symmetry directions KΓ and ΓL. Right panels: Momentum-dependent coupling constants for the two bands crossing the Fermi level. Spin-orbit coupling was taken into account in the calculations.*

In the general case, many phonon modes of different energies contribute to $\alpha^2 F_{\mathbf{k}\nu}(\omega)$ resulting in a broadened self-energy and kink structure. The coupling parameter is related to the slope of $\mathrm{Re}\Sigma$ at the Fermi energy, and the exact relation

$$\lambda_{\mathbf{k}\nu} = \left.\frac{\partial \mathrm{Re}\Sigma(\mathbf{k}\nu, \epsilon)}{\partial \epsilon}\right|_{\epsilon=\epsilon_F, T=0}, \tag{78}$$

holds. It has been used to extract the coupling parameter from measurements of the renormalized electronic bands.

Application of the first principles approach to a real system is exemplified for the case of lead [57]. Fig. 10 shows the results for the coupling constant of electronic states for two bands crossing the Fermi surface. One can observe that $\lambda_{\mathbf{k}\nu}$ can be significantly smaller or larger than the Fermi-surface average of $\lambda = 1.56$ discussed in Sec. 3.3. The variations partly reflect that the availability of intermediate states contributing to the renormalization depends on the binding energy and partly result from a momentum dependence of the EPC matrix elements.

Connection to experiment can be established by comparing the self-energy of states at the Fermi level. Fig. 11 shows data from angle-resolved photoemission spectroscopy experiments for the state of band #8 at the crossing with the Fermi level along the K-Γ direction. The calculations describe the data rather satisfactorily. For this state they predict a coupling constant of $\lambda_k = 1.79$, which is 15% larger than the Fermi-surface average.

The above-given analysis rests on a simplified solution of the Dyson equation which is justified as long as the coupling does not become too large. A generalized treatment has been presented by Eiguren *et al.* [59] that employs a self-consistent solution of the Dyson equation in the complex plane. They showed that for larger coupling the renormalization process becomes much more involved. It can lead to a complex structure of the electronic spectral function, indicating a break-down of the quasiparticle picture.
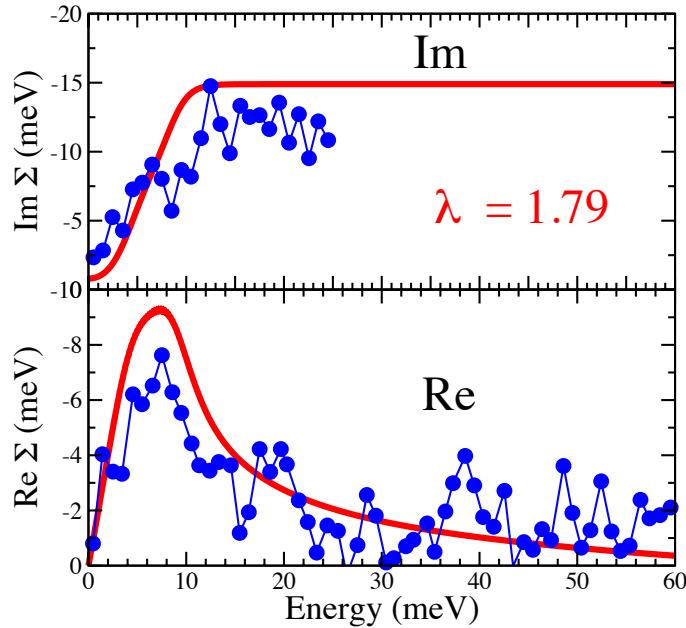
Fig. 11: *Electronic self-energy for Pb. Compared are calculated and measured results for the electronic state at the Fermi-surface crossing of band #8 along the $K\Gamma$ direction (see Fig. 10). Calculations (red lines) include spin-orbit coupling. Angle-resolved photoemission data (blue symbols) were taken from Reinert* et al. *[58].*

4   Summary

In this tutorial, I have given an introduction to the first principles approach to phonons and electron-phonon interaction within the linear-response framework of density functional theory, the so-called density functional perturbation theory. We have seen that adiabatic lattice vibrations are linked directly to electronic ground-state properties, and their properties can be calculated efficiently within the DFPT scheme. In contrast, electron-phonon coupling is a truly non-adiabatic property. Nevertheless, DFPT provides a simple way to quantify the screened electron-phonon vertex, which is one of the central quantities determining physical observables like phonon linewidth, electron renormalization, or phonon-mediated pairing interaction. This approach is valid as long as the electronic structure does not possess peculiarities on the energy scale of phonons.

This technique has been applied in recent years to a large variety of compounds. Its most common use was devoted to quantitative estimates of the pairing interaction for superconductors, providing valuable information about the basic question of the pairing mechanism. Measurements of quasiparticle renormalization are a more direct tool to gain information about the energy and momentum dependence of the electron-phonon vertex, and offer the possibility to check the accuracy of the DFPT predictions in greater detail. This route should be pursued more systematically in the future. A current challenge in this field is to incorporate more sophisticated treatments of electron correlations in order to extend applications to systems where strong correlations play a crucial role.

References

[1] M. Born and J.R. Oppenheimer, Ann. Physik **84**, 457 (1927)

[2] G.V. Chester and A. Houghton, Proc. Phys. Soc. **73**, 609 (1959)

[3] M. Born and K. Huang: *Dynamical Theory of Crystal Lattices*
    (Clarendon Press, Oxford, 1954)

[4] A.A. Maradudin, E.W. Montroll, G.H. Weiss, and I.P. Ipatova,
    in *Solid State Physics, Supplement 3* (Academic Press, New York, 1971), p. 1

[5] H. Boettger: *Principles of the Theory of Lattice Dynamics*
    (Physik Verlag, Weinheim, 1983)

[6] P. Hohenberg and W. Kohn, Phys. Rev. **136**, B 864 (1964)

[7] W. Kohn and L.J. Sham, Phys. Rev. **140**, A 1133 (1965)

[8] R.M. Dreizler and E.K.U. Gross:
    Density Functional Theory: An Approach to the Quantum Many-Body Problem
    (Springer-Verlag, Berlin, 1990)

[9] R.O. Jones and O. Gunnarsson, Rev. Mod. Phys. **61**, 689 (1989)

[10] R.G. Parr and W. Yang: *Density-Functional Theory of Atoms and Molecules*
     (Oxford University Press, New York, 1989)

[11] D.C. Langreth and M.J. Mehl, Phys. Rev. B **28**, 1809 (1983)

[12] J.P. Perdew, K. Burke, and M. Ernzerhof, Phys. Rev. Lett. **77**, 3865 (1996)

[13] J.P. Perdew, K. Burke, and M. Ernzerhof, Phys. Rev. Lett. **78**, 1396 (1997)

[14] J. Fritsch and U. Schröder, Phys. Rep. **309**, 209 (1999)

[15] M.T. Yin and M.L. Cohen, Phys. Rev. Lett. **45**, 1004 (1980)

[16] K. Kunc and R.M. Martin, J. Phys. (Paris) **42**, C6 (1981)

[17] K. Kunc and R.M. Martin, Phys. Rev. Lett. **48**, 406 (1982)

[18] M.T. Yin and M.L. Cohen, Phys. Rev. B **25**, 4317 (1982)

[19] W. Frank, C. Elsässer, and M. Fähnle, Phys. Rev. Lett. **74**, 1791 (1995)

[20] G. Kresse, J. Furthmüller, and J. Hafner, Europhys. Lett. **32**, 729 (1995)

[21] K. Parlinski, Z.Q. Li, and Y. Kawazoe, Phys. Rev. Lett. **78**, 4063 (1997)

[22] G.J. Ackland, M.C. Warren, and S.J. Clark, J. Phys. Condens. Matt. **9**, 7861 (1997)

[23] R.P. Feynman, Phys. Rev. **56**, 340 (1939)

[24] M.S. Hybertsen and S.G. Louie, Phys. Rev. B **35**, 5585 (1987)

[25] S.L. Adler, Phys. Rev. **126**, 413 (1962)

[26] N. Wiser, Phys. Rev. **129**, 62 (1963)

[27] R.M. Pick, M.H. Cohen, and R.M. Martin, Phys. Rev. B **1**, 910 (1970)

[28] R. Resta, Adv. Solid State Phys. **25**, 183 (1985)

[29] W.R. Hanke, Phys. Rev. B **8**, 4585 (1973)

[30] N.E. Zein, Sov. Phys. Solid State **26**, 1825 (1984)

[31] D.K. Blat, N.E. Zein, and V.I. Zinenko, J. Phys. Condens. Matt. **3**, 5515 (1991)

[32] N.E. Zein, Phys. Lett. A **161**, 526 (1992)

[33] S. Baroni, P. Giannozzi, and A. Testa, Phys. Rev. Lett. **58**, 1861 (1987)

[34] P. Giannozzi, S. de Gironcoli, P. Pavone, and S. Baroni, Phys. Rev. B **43**, 7231 (1991)

[35] S. Baroni, S. de Gironcoli, A. Dal Corso, and P. Giannozzi,
Rev. Mod. Phys. **73**, 515 (2001)

[36] X. Gonze and J.-P. Vigneron, Phys. Rev. B **39**, 13120 (1989)

[37] X. Gonze, Phys. Rev. A **52**, 1086 (1995)

[38] X. Gonze, Phys. Rev. A **52**, 1096 (1995)

[39] S. de Gironcoli, Phys. Rev. B **51**, 6773 (1995)

[40] A. Dal Corso, J. Phys.: Condens. Matter **20**, 445202 (2008)

[41] M.J. Verstraete, M. Torrent, F. Jollet, G. Zérah, and X. Gonze, Phys. Rev. B **78**, 045119 (2008)

[42] G. Grimvall: *The Electron–Phonon Interaction in Metals*
in E. Wohlfarth (ed.): *Selected Topics in Solid State Physics*
(North-Holland, New York, 1981)

[43] R. Heid, K.-P. Bohnen, I.Yu. Sklyadneva, and E.V. Chulkov,
Phys. Rev. B **81**, 174527 (2010)

[44] F. Giustino, M.L. Cohen, and S.G. Louie, Phys. Rev. B **76**, 165108 (2007)

[45] M. Calandra, G. Profeta, and F. Mauri, Phys. Rev. B **82**, 165111 (2010)

[46] P.B. Allen, Phys. Rev. B **6**, 2577 (1972)

[47] F. Weber, S. Rosenkranz, L. Pintschovius, J.-P. Castellan, R. Osborn, W. Reichardt, R. Heid, K.-P. Bohnen, E.A. Goremychkin, A. Kreyssig, K. Hradil, and D. Abernathy, Phys. Rev. Lett. **109**, 057001 (2012)

[48] A.M. Saitta, M. Lazzeri, M. Calandra, and F. Mauri, Phys. Rev. Lett. **100**, 226401 (2008)

[49] J. Bardeen, L.N. Cooper, and J.R. Schrieffer, Phys. Rev. **108**, 1175 (1957)

[50] D.J. Scalapino: *The Electron-Phonon Interaction and Strong-Coupling Superconductors* in R.D. Parks (ed.): *Superconductivity*, Vol. 1 (Dekker, New York, 1969)

[51] G.M. Eliashberg, Zh. Eksp. Fiz. **38**, 966 (1960); Engl. Transl.: Sov. Phys. – JETP **11**, 696 (1960)

[52] P.B. Allen and B. Mitrović, Solid State Physics **37**, 1 (1982)

[53] B.N. Brockhouse, T. Arase, G. Cagliotti, K.R. Rao, and A.D.B. Woods, Phys. Rev. **128**, 1099 (1962)

[54] W.L. McMillan and J.M. Rowell: *Tunneling and Strong-Coupling Superconductivity* in R.D. Parks (ed.): *Superconductivity*, Vol. 1 (Dekker, New York, 1969)

[55] J. Geerk, R. Schneider, G. Linker, A.G. Zaitsev, R. Heid, K.-P. Bohnen, and H.v. Löhneysen, Phys. Rev. Lett. **94**, 227005 (2005)

[56] Ph. Hofmann, I.Yu. Sklyadneva, E.D.L Rienks, and E.V. Chulkov, New J. Phys. **11**, 125005 (2009)

[57] I.Yu. Sklyadneva, R. Heid, P.M. Echenique, K.-P. Bohnen, and E.V. Chulkov, Phys. Rev. B **85**, 155115 (2012)

[58] F. Reinert, B. Eltner, G. Nicolay, D. Ehm, S. Schmidt, and S. Hüfner, Phys. Rev. Lett. **91**, 186406 (2003); *ibid* Phys. Rev. Lett. **92**, 089904 (2004) (Erratum)

[59] A. Eiguren, C. Ambrosch-Draxl, and P.M. Echenique, Phys. Rev. B **79**, 245103 (2009)